Development and Implementation of a Composite Material Shell-Element Model

Tobias Achstetter, Paul Du Bois, Kelly Carney, Cing-Dao Kan
George Mason University
Allen Sheldon
Honda R&D Americas
Sheng Dong
The Ohio State University
Gunther Blankenhorn
Livermore Software Technology Corporation

Abstract

While the response to loading of traditional engineering materials, such as plastics and steel, is well understood and can be simulated accurately, designers of composite structures still rely heavily on physical testing of components to ensure the requirements of load bearing capabilities are met.

The majority of composite material models that have been developed rely on non-physical material parameters that have to be calibrated in extensive simulations. A predictive model, based on physically meaningful input, is currently not available.

The developed orthotropic material model includes the ability to define tabulated hardening curves for different loading directions with strain-rate and temperature dependency. Strain-rate dependency was achieved by coupling the theories of viscoelasticity and viscoplasticity to allow for rate dependency in both the elastic and plastic regions of the material deformation. A damage model was implemented, where a reduction of stiffness and stress degradation in the individual material directions can be tracked precisely. Modeling of failure and Finite Element erosion was achieved by implementing a new strain-based generalized tabulated failure criterion, where failure strains can be precisely defined for specific states of stresses. Composite materials are generally used in a layup of plies with different fiber directions. These individual plies are very thin, which leads to impractically small mesh sizes when modeled with three dimensional solid elements. The developed material model is, therefore, made available for shell elements.

The presented material model is a step towards the goal of a truly predictive material model for composite materials.

Strain-rate dependency

This paper describes the theory of the newly developed orthotropic viscoelastic viscoplastic material model for composites. It was implemented into LS-DYNA® as MAT213 for shell elements.

Figure 1 shows three different types of viscous material behaviors. Viscoelastic behavior, as shown in Figure 1a, is typical for polymers and rubbers. This type of material model is used when non-linear behavior without permanent deformation occurs and rate dependency in the elastic region should be modeled.
Rate dependency in metals is commonly modeled with a viscoplasticity model, as depicted in Figure 1b. Both the yield stress of the material and the hardening can be rate-dependent while the elastic modulus stays constant at different loading rates.

Fiber reinforced composites, on the other hand, exhibit characteristics of both viscoelasticity and viscoplasticity with rate dependencies in both the elastic and plastic regions (Figure 1c). The presented material model allows, therefore, for both viscoelastic and viscoplastic behavior in combination.

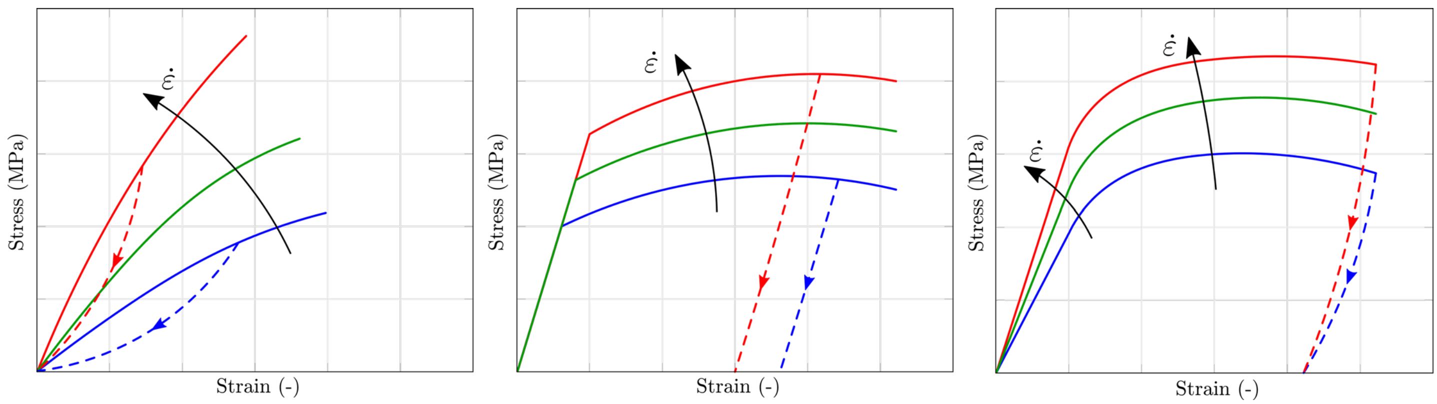

a) Viscoelasticity *b) Viscoplasticity* *c) Viscoelasticity and -plasticity*

Figure 1: Forms of viscous behavior

Viscoelasticity

The theory of viscoelasticity is a well-established method to mathematically describe the material behavior of polymers that exhibit both viscous and elastic characteristics when undergoing deformations. Viscous materials resist strain dependent on time, while elastic materials return to their original state once the loading is removed [1]. Figure 1a shows the typical response to loading of a viscoelastic polymer. An increase in strain-rate leads to an increase in the Young's modulus. When the stress on the material is removed, it returns to its original state with no permanent deformation.

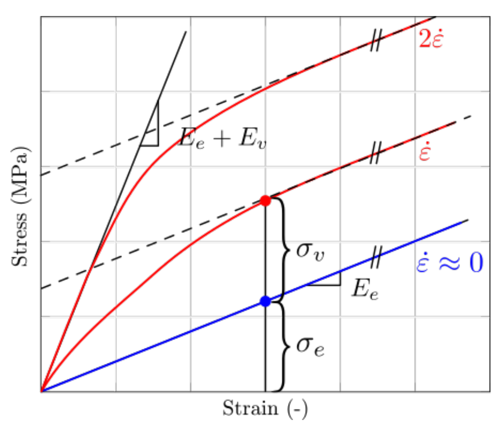

Figure 2: Viscoelastic behavior at different rates

Figure 2 shows example results of viscoelastic behavior at different constant strain-rates that can be described by the differential equation as follows:

$$\dot{\sigma} + \frac{E_v}{\eta}\sigma = (E_e + E_v)\dot{\varepsilon} + \frac{E_e E_v}{\eta}\varepsilon \tag{1}$$

For a very low strain-rate, the slope of the stress vs. strain response is equal to the equilibrium stiffness E_e and follows the blue curve, while for a high rate the slope approaches $(E_e + E_v)$.
After simplifications and numerical integration, assuming a constant strain-rate $\dot{\varepsilon}$ and stiffness E_v during one time step, the viscous stress at time step t^{n+1} can be computed:

$$\sigma_v\left(t^{n+1}\right) = e^{-\beta\Delta t}\sigma_v(t^n) + E_v\dot{\varepsilon}^{n+\frac{1}{2}}\frac{1-e^{-\beta\Delta t}}{\beta} \tag{2}$$

Non-linear Viscoelasticity

To allow for an arbitrary tabulated relationship between the Young's modulus and the total strain-rate, the classical linear viscoelasticity described in the previous Section, is replaced by a non-linear viscoelastic model. For this material model, the Young's modulus is derived from the tabulated stress-strain data for every current strain-rate value and, therefore, the stiffness is a function of the strain-rate $E_v(\dot{\varepsilon})$. By assuming a constant β, Equation 2 can be modified to compute the viscous stress and to allow for the non-linear spring $E_v(\dot{\varepsilon})$:

$$\sigma_v\left(t^{n+1}\right) = e^{-\beta\Delta t}\sigma_v(t^n) + E_v(\dot{\varepsilon}^{n+\frac{1}{2}})\dot{\varepsilon}^{n+\frac{1}{2}}\frac{1-e^{-\beta\Delta t}}{\beta} \tag{3}$$

The choice of a constant decay coefficient allows matching the initial slope of the dynamic stress-strain curves with a single input variable. At large strains this model has limited flexibility to match the measured data, however, at larger strains the viscoplastic fraction of the material law (described in the following Section) is expected to dominate the response.

Viscoplasticity

The theory of viscoplasticity is applied to model the irreversible and time-dependent deformation of materials. In contrast to a rate-independent plastic material, a viscoplastic material can undergo a creep flow as a function of time. Creep describes how a material slowly deforms permanently under a constant stress. Figure 3c shows an example of a constant stress load with the corresponding creep in the strain response in Figure 3a.
Similarly, for a constant strain load (Figure 3b) a viscoplastic material will respond with stress relaxation (Figure 3d) and, consequently, a continuous decay of the stress over time.

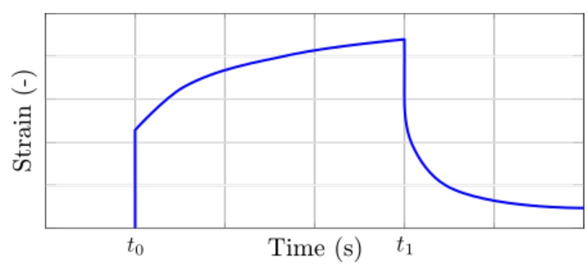

a) Creep strain

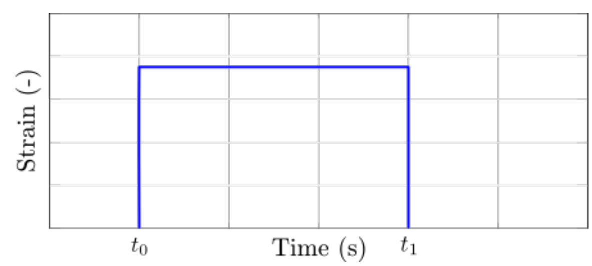

b) Relaxation strain

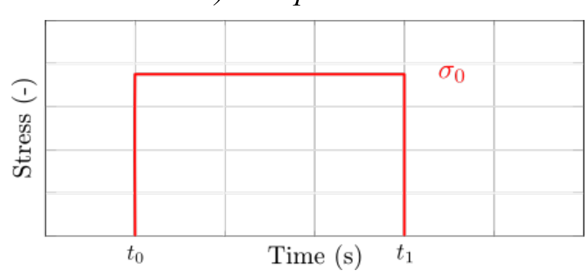

c) Creep stress

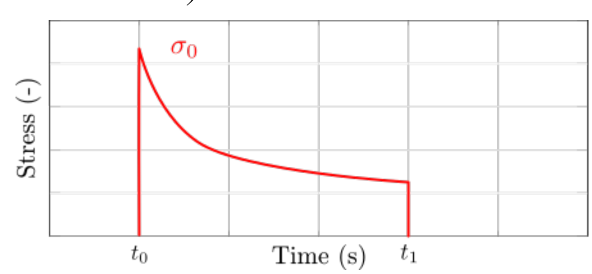

d) Relaxation stress

Figure 3: Creep and relaxation

Essential for a viscoplasticity model is the decomposition of the total strain into the sum of a recoverable elastic and a permanent plastic component:

$$\varepsilon = \varepsilon_{el} + \varepsilon_p \tag{4}$$

where the elastic strain ε_{el} is related to the elastic stress by means of the standard linear elastic constitutive relation.

In the example of one-dimensional plasticity theory, the existence of an elastic domain, for which the material behavior is purely elastic, is defined by a yield stress. While the stress is lower than the yield stress σ_y, the material response is linear elastic. This yield stress can be dependent on different variables, such as the plastic strain ε_p, the plastic strain-rate $\dot{\varepsilon}_p$, where rate effects should be captured, and/or the temperature T in temperature-dependent models:

$$\sigma_y = f\left(\varepsilon_p, \dot{\varepsilon}_p, T\right) \tag{5}$$

In addition to the elastic constitutive relation, a flow rule is needed to describe the permanent plastic deformation once the yield stress is exceeded. For a loading under tension ($\sigma > 0$) the plastic strain-rate should be positive (stretching) and negative under compression ($\sigma < 0$). The plastic flow rule for a uniaxial model can thus be established as follows [2]:

$$\dot{\varepsilon}_p = \dot{\lambda}\ sign(\sigma) \tag{6}$$

Temperature dependency

Mechanical properties of polymeric materials are temperature sensitive, with the effect increasing as the glass transition temperature is approached. For example, the yield stress of a polymer at the glass transition temperature tends to zero [3]. For many applications it is important to model these effects accurately. In the following text, adiabatic heating effects due to plastic work will be discussed.

When metal deforms plastically, a rise in temperature of the material can be measured. Explanations of this phenomenon discuss the process of hardening due to phase changes of the material and in turn changes of the internal energy of the material [4]. By comparing the heat equivalent of the work done and the measured heat during the deformation, a change in internal energy of the material can be verified. In metals, generally between 5 and 15% of the work done is spent on phase changes of the material, while the majority is converted to heat and leads to a rise in temperature of the specimen. This temperature rise also depends on the rate of loading. If the generated heat has time to conduct away, little temperature rise can be measured (isothermal conditions). When the time scales of the experiment are very short, adiabatic conditions occur and the temperature can rise noticeably. Rittel discussed this phenomenon for polymers [6]. Trojanowski et al. [3] used infrared detectors to monitor temperature rise in epoxy specimens tested in a split Hopkinson pressure bar. The achieved strain-rate was $2500\frac{1}{s}$ and the measured temperature rise for a specific epoxy reached 40°C.

According to Taylor and Quinney, the adiabatic rise in temperature in a material due to plastic work (W_p) can be calculated as follows [5]:

$$d\dot{T} = \frac{\beta_t}{C_p \rho} d\dot{W}_p \tag{8}$$

where $\dot{T}$ is the change in temperature, β_t is the Taylor–Quinney coefficient that represents the proportion of plastic work converted into heat, ρ is the density, and C_p is the specific heat at constant pressure.

With the equivalence of plastic work (Equation 8), Equation 9 can be expressed in terms of the flow rule coefficient and plastic multiplier as follows in Equation 10.

$$\dot{W}_p = \boldsymbol{\sigma} : \dot{\boldsymbol{\varepsilon}}_p = \boldsymbol{\sigma} : \dot{\lambda}\frac{\partial h}{\partial \boldsymbol{\sigma}} = h\dot{\lambda} \tag{9}$$

$$\dot{T} = \frac{\beta_t}{C_p \rho} h\dot{\lambda} \tag{10}$$

With the rise in temperature, the polymer matrix material softens, decreasing the yield stress of the material in matrix dominated material directions.

Damage

When a composite material is loaded, irreversible micro-cracks and cavities can form. These defects cause stiffness degradation in the composite [7]. To capture this softening of the stress-strain response, the material model is enhanced by a damage model. Strain equivalence is assumed, meaning that in both the true and effective stress space, elastic and plastic strains are the same [8]. This allows for the damage calculations to be uncoupled and independent of the plasticity algorithm that takes place in the effective stress space. The effective (undamaged) stresses are related to the true (damaged) stresses by the damage tensor $\boldsymbol{M}$, as shown in Equation 11 [9]:

$$\begin{bmatrix}\sigma_{11}\\ \sigma_{22}\\ \sigma_{12}\end{bmatrix} = \begin{bmatrix}M_{11} & 0 & 0\\ 0 & M_{22} & 0\\ 0 & 0 & M_{44}\end{bmatrix}\begin{bmatrix}\sigma_{11_{eff}}\\ \sigma_{22_{eff}}\\ \sigma_{12_{eff}}\end{bmatrix} \tag{11}$$

The use of a diagonal damage tensor suggests that loading in a specific material direction leads to a reduction in stiffness in this direction only. Experimental research in composites suggests that a load in one material direction can lead to damage in another material direction. The in-plane shear modulus, for example, can decrease with increasing tensile load due to transverse cracking of the matrix [10]. Similarly, the transverse stiffness can be reduced due to damage accumulation in shear loading [11]. These effects are accounted for by including the coupling terms between material directions in the components of the damage tensor.
These are computed as follows in Equations 12 to 16 [12]. The superscripts of the damage coefficients d denote in which direction the damage is occurring, while the subscripts specify which loading direction caused the damage. For example, $\mathrm{d}_{11_C}^{11_T}$ would be the coupled damage coefficient for damage in tension 1-direction due to loading in compression 1-direction. Depending on whether the current state of stress is positive or negative, the corresponding component of the damage tensor is computed using the coefficients for tension or compression. This can be viewed for 1-direction tension in Equation 12 or 1-direction compression in Equation 13.

$$\sigma_{11} > 0: \quad M_{11} = \left(1 - d_{11_T}^{11_T}\right)\left(1 - d_{11_C}^{11_T}\right)\left(1 - d_{22_T}^{11_T}\right)\left(1 - d_{22_C}^{11_T}\right)\left(1 - d_{12}^{11_T}\right) \tag{12}$$

$$\sigma_{11} < 0: \quad M_{11} = \left(1 - d_{11_T}^{11_C}\right)\left(1 - d_{11_C}^{11_C}\right)\left(1 - d_{22_T}^{11_C}\right)\left(1 - d_{22_C}^{11_C}\right)\left(1 - d_{12}^{11_C}\right) \tag{13}$$

$$\sigma_{22} > 0: \quad M_{22} = \left(1 - d_{11_T}^{22_T}\right)\left(1 - d_{11_C}^{22_T}\right)\left(1 - d_{22_T}^{22_T}\right)\left(1 - d_{22_C}^{22_T}\right)\left(1 - d_{12}^{22_T}\right) \tag{14}$$

$$\sigma_{22} < 0: \quad M_{22} = \left(1 - d_{11_T}^{22_C}\right)\left(1 - d_{11_C}^{22_C}\right)\left(1 - d_{22_T}^{22_C}\right)\left(1 - d_{22_C}^{22_C}\right)\left(1 - d_{12}^{22_C}\right) \tag{15}$$

$$M_{44} = \left(1 - d_{11_T}^{22_C}\right)\left(1 - d_{11_C}^{22_C}\right)\left(1 - d_{22_T}^{22_C}\right)\left(1 - d_{22_C}^{22_C}\right)\left(1 - d_{12}^{22_C}\right) \tag{16}$$

The damage terms are defined as a function of strain by the user. In the initialization phase, the damage versus strain curves are transformed to damage versus plastic strain curves to track damage accumulation in the different directions independently. The user provided true (damaged) stress versus strain input curves in the individual directions are converted based on these damage versus strain curves to effective (undamaged) stress versus effective plastic strain curves. This separates damage effects and plasticity in the algorithm. For this conversion, only the plastic strain in the loading direction, for which the stress versus strain curves was defined, is used.
The plastic strains in terms of the plastic multiplier, plastic potential, and the stresses for the normal strains are shown in Equation 17:

$$\dot{\varepsilon}_{11_p} = \frac{\dot{\lambda}}{2h}(2H_{11}\sigma_{11} + 2H_{12}\sigma_{22}) \qquad \dot{\varepsilon}_{22_p} = \frac{\dot{\lambda}}{2h}(2H_{12}\sigma_{11} + 2H_{22}\sigma_{22}) \tag{17}$$

For the two special cases of uniaxial tension or compression in the 1- and 2-direction, this leads to the following plastic strains:

$$\begin{bmatrix}\sigma_{11} & 0\\ 0 & 0\end{bmatrix} \Rightarrow \begin{cases} \dot{\varepsilon}_{11_p} = \frac{\dot{\lambda}}{2h}(2H_{11}\sigma_{11}) \\ \dot{\varepsilon}_{22_p} = \frac{\dot{\lambda}}{2h}(2H_{12}\sigma_{11}) \end{cases} \qquad \begin{bmatrix}0 & 0\\ 0 & \sigma_{22}\end{bmatrix} \Rightarrow \begin{cases} \dot{\varepsilon}_{11_p} = \frac{\dot{\lambda}}{2h}(2H_{12}\sigma_{22}) \\ \dot{\varepsilon}_{22_p} = \frac{\dot{\lambda}}{2h}(2H_{22}\sigma_{22}) \end{cases} \tag{18}$$

The transversal plastic strains caused by the longitudinal stress components will add to the longitudinal damage if coupled damage terms are defined. This then leads to the output curves not matching the user defined input, as during the curve conversion from true (damaged) stress to effective (undamaged) stress only the longitudinal uncoupled damage in this direction was considered. To counteract this issue, "corrected plastic strains" are defined.
Equation 19 shows the corrected plastic strains to only consider damage in loading direction:

$$\dot{\varepsilon}_{11_{pc}} = \frac{\dot{\lambda}}{2h}\left(2H_{11}\sigma_{11}\right) \qquad \dot{\varepsilon}_{22_{pc}} = \frac{\dot{\lambda}}{2h}\left(2H_{22}\sigma_{22}\right) \qquad \dot{\varepsilon}_{12_{pc}} = \frac{\dot{\lambda}}{2h}\left(H_{44}\sigma_{12}\right) \tag{19}$$

A formulation based on these corrected plastic strains guarantees that the output curves match the input curves for uniaxial load cases.

Generalized Tabulated Failure Criterion

Failure of material in finite element simulations is generally handled by removing elements from the simulation where stresses or strains are determined to have exceeded a failure criterion. In crash, crush or ballistic impact simulations of composites, however, removing elements from the simulation once a failure criterion is satisfied in only one material direction does lead to non-physical behavior. Consider loading a unidirectional composite in tension 2-direction until matrix cracks or fiber-matrix debonding occurs. In this uniaxial test, the material would now be considered to have "failed". In reality, however, many if not most fibers might still be intact, and the material can still take load when reloaded in the fiber direction. Following traditional failure models, elements in a finite element simulation would have been eroded and load bearing capabilities in all directions would be lost. In the following, a flexible erosion criterion for composites is introduced.

The erosion criterion can be used both as a traditional composite failure model, or to erode highly deformed elements that have lost most of their load bearing capabilities in the different material directions due to damage. Damage and erosion are therefore handled independent from each other. This allows the use of the damage model to progressively degrade the material in different directions and the Generalized Tabulated Failure Criterion to erode the elements once damage has sufficiently decreased the ability of the material to take any further loads. To define when erosion should occur, a failure surface is introduced. This surface describes a surface in stress or strain space for which the material fails. If the stress state is within the surface, failure does not occur. Once the stress or strain state lies on or beyond the failure surface, the material fails. In traditional failure models, mathematical functions describe the shape of this surface. This restricts the shape of the surface and failure of a composite may or may not be accurately modeled. To overcome this restriction, a tabulated approach similar to the one described by Goldberg et al. [13] is used.

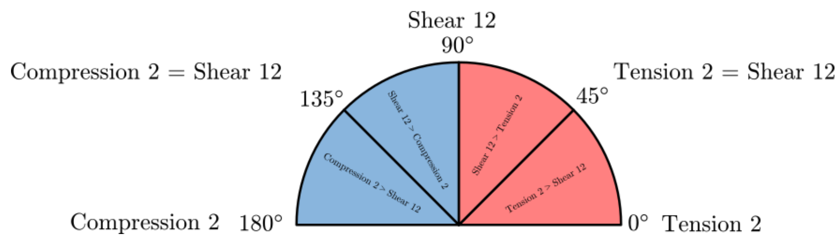

Figure 4: Angle values for specific states of stress

To describe a state of plane stress uniquely, two independent variables are necessary. In the following approach, an angle is used as the first independent variable describing the location of a point in the σ_{22}-σ_{12} plane:

$$\theta = cos^{-1}\left(\frac{\sigma_{22}}{\sqrt{\sigma_{22}^2 + \sigma_{12}^2}}\right) \tag{20}$$

The meaning of this angle in bi-axial loading is visualized in Figure 4. In the case of pure Tension 2-direction loading ($\sigma_{12} = 0$ and $\sigma_{22} > 0$) the computed angle θ is zero, whereas in the case of pure Shear 12-direction loading ($\sigma_{22} = 0$) the computed angle is 90°.

As the second independent variable, the value of the stress in 1-direction σ_{11} is used. These two independent variables describe the location of a point on the failure surface, while a dependent variable defines the magnitude of said failure surface. In contrast to Goldberg et al. [13], the dependent variable of choice is an equivalent strain, as defined in Equation 21:

$$\varepsilon_{eq} = \sqrt{\varepsilon_{11}^2 + \varepsilon_{22}^2 + 2\varepsilon_{12}^2} \tag{21}$$

This equivalent strain is then compared with the user-defined value of an equivalent failure strain ε_{fail} for the given angle and shear stress.

$$d = \frac{\varepsilon_{eq}}{\varepsilon_{fail}} \tag{22}$$

For $\mathrm{d} \geq 1$ the element fails and is eroded. The possibility to define a discrete value for any state of plane stress allows one to include actual experimental data to construct the failure surface. Failure variables for states of stress where the user cannot obtain experimental values can be calculated using traditional analytical failure models or numerical experiments.

Figure 5 shows an example of such a failure surface. The in-plane axis “Fiber direction stress” and “Angle” describe the state of stress the element undergoes, while the out-of-plane axis “Equivalent failure strain” describes the magnitude of strains at which the element is eroded.

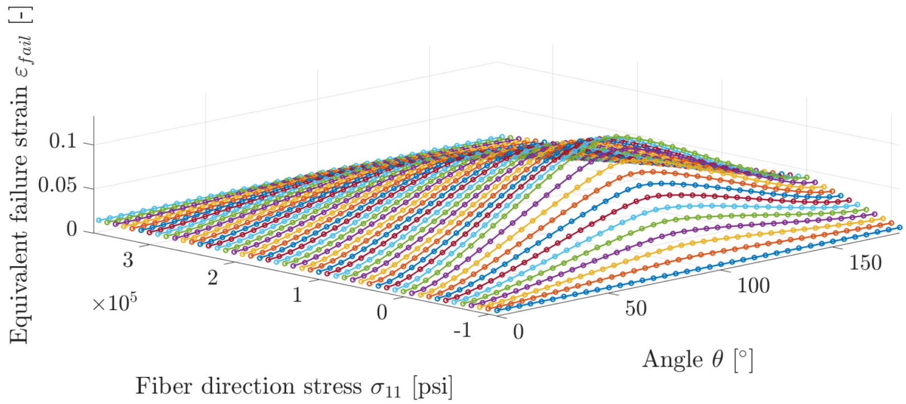

Figure 5: Failure surface

Robustness

In certain loading conditions and for specific user input, the non-associated flow rule might not be able to find a solution that returns the trial stress to the yield surface.
To visualize this issue, the following input was used:

- Flow rule coefficients: $\mathrm{H}_{11} = 0.01$, $\mathrm{H}_{22} = 1.0$.
- Yield stresses: $\sigma_{11y_T} = 1430$, $\sigma_{22y_T} = 42$, $\sigma_{11y_C} = 510$, $\sigma_{22y_C} = 145$, $\sigma_{12y} = 63$, $\sigma_{45y} = 68$

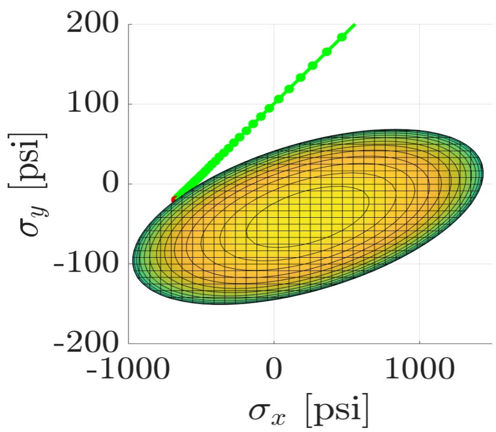

a) Yield surface full view in x-y-plane

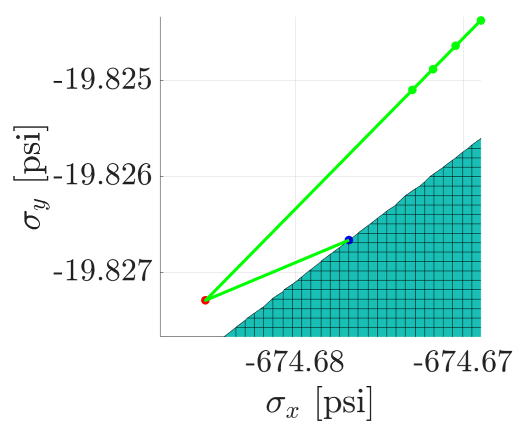

b) Yield surface zoomed

Figure 6: Yield surface with no solution in non-associated flow

The yield stresses result in a yield surface, as shown in Figure 6a, where a projected view on the x-y-plane is shown. Figure 6b shows the same yield surface zoomed in on the initial stress state (blue circle) and the elastic trial stress (red circle). Due to the chosen flow rule coefficients, the plasticity algorithm is searching for possible stress states that should lie within the yield surface along the green line, with the estimates computed by the plasticity algorithm shown as green circles. None of the computed stress estimates lie within the yield surface and, therefore, no solution in the non-associated case with the chosen flow rule coefficients can be found. The problem lies in the angle between the yield surface and the flow direction being greater than 90°. Figure 7 visualizes a case where this angle Φ is greater than 90° and so the flow direction points away from the yield surface.

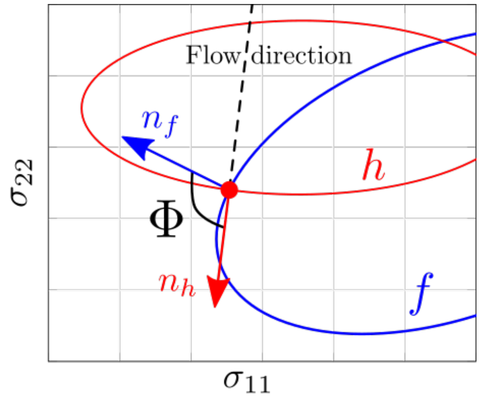

Figure 7: Angle between flow and yield surface

When the non-associated flow rule is not able to find a solution on the yield surface, the flow rule is first modified to be associated. The plastic work equation is changed to use the yield function instead of the plastic potential, where the variable k is introduced to keep the equation at consistent dimensions:

$$\dot{W}_p = \boldsymbol{\sigma}_t : \dot{\varepsilon}_p = \boldsymbol{\sigma}_t : \dot{\lambda}\frac{\partial h}{\partial \boldsymbol{\sigma}_t} = \boldsymbol{\sigma}_t : \dot{\lambda}^{mod}\frac{\partial f}{\partial \boldsymbol{\sigma}_t}k \tag{23}$$

where variables h, and k are in units of stress while the yield function f is dimensionless. It is now ensured, that the scalar plastic multiplier increment $\dot{\lambda}$ stays unchanged in Equation 23 and, therefore, the following should be true:

$$\dot{\lambda}^{mod} = \dot{\lambda} \tag{24}$$

Scale factor k can then be computed to ensure Equation 24 holds true.

$$\boldsymbol{\sigma}_t : \frac{\partial h}{\partial \boldsymbol{\sigma}_t} = \boldsymbol{\sigma}_t : \frac{\partial f}{\partial \boldsymbol{\sigma}_t}k \qquad \Rightarrow \qquad k = \frac{\boldsymbol{\sigma}_t : \frac{\partial h}{\partial \boldsymbol{\sigma}_t}}{\boldsymbol{\sigma}_t : \frac{\partial f}{\partial \boldsymbol{\sigma}_t}} \tag{25}$$

Consequently, Equation 23 simplifies to:

$$\dot{W}_p = \boldsymbol{\sigma}_t : \dot{\lambda}\frac{\partial f}{\partial \boldsymbol{\sigma}_t}\frac{\boldsymbol{\sigma}_t : \frac{\partial h}{\partial \boldsymbol{\sigma}_t}}{\boldsymbol{\sigma}_t : \frac{\partial f}{\partial \boldsymbol{\sigma}_t}} \tag{26}$$

This effectively modifies the direction of the plastic strain increment without changing the magnitude of the plastic strain increment. In many situations where the angle between the flow direction and yield surface could lead to the plasticity algorithm not finding a solution, modification of the flow rule to be associated can prevent this issue. In some rare cases in complex loading conditions, even associated flow in anisotropic materials might not allow for the plasticity algorithm to find a valid stress state on the yield surface in the direction of plastic flow. To increase the robustness of the material model, error terminations due to this problem must be prevented.

For the very rare instances where both the non-associated flow rule and associated flow rule fail to find a solution, the flow direction is changed to project radially towards the origin of the stress space to ensure a solution within the yield surface is found. Instead of projecting non-associated towards $-\boldsymbol{C}\frac{\partial h}{\partial \boldsymbol{\sigma}_t}$, the projection from the trial stress towards the origin is in the direction of $-\boldsymbol{\sigma}_t$, as shown in Equation 27:

$$\boldsymbol{\sigma}^{n+1} = \boldsymbol{\sigma}_t^{n+1} - \boldsymbol{C}\Delta\lambda\frac{\partial h}{\partial \boldsymbol{\sigma}_t} \qquad \Rightarrow \qquad \boldsymbol{\sigma}^{n+1} = \boldsymbol{\sigma}_t^{n+1} - \Delta\lambda\boldsymbol{\sigma}_t n = \boldsymbol{\sigma}_t^{n+1} - \boldsymbol{C}\boldsymbol{C}^{-1}\Delta\lambda\boldsymbol{\sigma}_t n \tag{27}$$

where n ensures that the plastic multiplier keeps the same length as in the non-associated case.

Similar to Equation 23, the scale factor n can then be computed from the plastic work equation:

$$\dot{W}_p = \boldsymbol{\sigma}_t : \dot{\varepsilon}_p = \boldsymbol{\sigma}_t : \dot{\lambda}\frac{\partial h}{\partial \boldsymbol{\sigma}_t} = \boldsymbol{\sigma}_t : \dot{\lambda}\boldsymbol{C}^{-1}\boldsymbol{\sigma}_t n \tag{28}$$

$$n = \frac{\boldsymbol{\sigma}_t : \frac{\partial h}{\partial \boldsymbol{\sigma}_t}}{\boldsymbol{\sigma}_t : \boldsymbol{C}^{-1}\boldsymbol{\sigma}_t} \tag{29}$$

And therefore Equation 28 simplifies to:

$$\dot{W}_p = \boldsymbol{\sigma}_t : \dot{\lambda}\boldsymbol{C}^{-1}\boldsymbol{\sigma}_t \frac{\boldsymbol{\sigma}_t : \frac{\partial h}{\partial \boldsymbol{\sigma}_t}}{\boldsymbol{\sigma}_t : \boldsymbol{C}^{-1}\boldsymbol{\sigma}_t} \tag{30}$$

This change of the plastic flow direction can be physically expressed by deriving the flow rule coefficients and therefore plastic Poisson's ratios that this modification produces. For the case of radial return, from Equation 28 follows that:

$$\frac{\partial h}{\partial \boldsymbol{\sigma}_t} = \boldsymbol{C}^{-1}\boldsymbol{\sigma}_t n \;\Rightarrow\; \boldsymbol{C}\frac{\partial h}{\partial \boldsymbol{\sigma}_t} = \boldsymbol{I}\boldsymbol{\sigma}_t n \;\Rightarrow\; \boldsymbol{C}\boldsymbol{H}\frac{1}{h_t}\boldsymbol{\sigma}_t = \boldsymbol{I}\boldsymbol{\sigma}_t n \;\Rightarrow\; \boldsymbol{C}\boldsymbol{H} = \boldsymbol{I}nh_t \tag{31}$$

where **I** is a 3x3 identity matrix.
Equation 31 can now be expressed in tensor notation:

$$\begin{bmatrix} c_{11} & c_{12} & 0 \\ c_{12} & c_{22} & 0 \\ 0 & 0 & c_{44} \end{bmatrix} \begin{bmatrix} H_{11} & H_{12} & 0 \\ H_{12} & H_{22} & 0 \\ 0 & 0 & H_{44} \end{bmatrix} = nh_t \begin{bmatrix} 1 & 0 & 0 \\ 0 & 1 & 0 \\ 0 & 0 & 1 \end{bmatrix} \tag{32}$$

Two equations of this system can be written as:

$$c_{12}H_{11} + c_{22}H_{12} = 0 \quad \Rightarrow \quad \frac{c_{12}}{c_{22}} = -\frac{H_{12}}{H_{11}} = \nu_{12}^p \tag{33}$$

$$c_{12}H_{22} + c_{11}H_{12} = 0 \quad \Rightarrow \quad \frac{c_{12}}{c_{11}} = -\frac{H_{12}}{H_{22}} = \nu_{21}^p \tag{34}$$

With the projection operator [14], the ratios of the two-dimensional stiffness matrix coefficients are calculated as follows:

$$\frac{c_{12}}{c_{22}} = \frac{q_{12} - \frac{q_{13}q_{23}}{q_{33}}}{q_{22} - \frac{q_{23}q_{23}}{q_{33}}} \tag{35}$$

$$\frac{c_{12}}{c_{11}} = \frac{q_{12} - \frac{q_{13}q_{23}}{q_{33}}}{q_{22} - \frac{q_{23}q_{23}}{q_{33}}} \tag{36}$$

where the factors q_{ij} are the components of the three-dimensional stiffness matrix. From Equations 35 and 36 then follows through simplifications that:

$$\frac{c_{12}}{c_{22}} = \nu_{12} \tag{37}$$

$$\frac{c_{12}}{c_{11}} = \nu_{21} \tag{38}$$

Using Equations 33, 34 and 37, 38, in the case of radial return the plastic Poisson's ratios, that can be derived from the modified radial flow surface, are equal to the elastic Poisson's ratios: $\nu_{12} = \nu_{12}^{p}$ and $\nu_{21} = \nu_{21}^{p}$.
The imposed plastic Poisson's ratios, that are assumed during the radial return, do therefore not lead to unreasonable values.
Both the solution obtained using associated flow and the radial return are a deviation from the non-associated theory that is utilized in the default case. However, an error termination of the simulation in the rare cases where the non-associated flow is not able to produce a valid solution is both not acceptable and not practical in industry scale simulations.
During a simulation, the material subroutine is entered for every integration point at every timestep. For example, in a ballistic impact simulation conducted using the new material model, a composite plate was modeled with 396,508 fully integrated elements with four integration points in-plane and two integration points through the thickness. The total number of integration points in the example simulation was, therefore, 3.172 million. The same ballistic impact simulation was then conducted using four different timestep scale factors (TSSFAC) ranging from 0.6 to 0.9. The timestep scale factor provides an option to scale the calculated timestep that is computed based on material parameters and element size to insure stability in the explicit integration solution.
Table 1 lists the statistics of the four simulations regarding occurrences of associated flow and radial return. Accumulated, approximately between 116 and 173 billion times a stress state was computed by the material model, depending on the timestep scale factor. With increasing scale factors from 0.7 to 0.9, the occurrences of both associated flow and radial return increased as well. In this particular case, the ideal TSSFAC of the four cases was 0.7 with the lowest occurrences of both associated flow and radial return. For a scale factor of 0.7, associated flow was used in 1.86 million cases (1 in ~80,000).
Changing from non-associated flow to associated flow does change the behavior of the model in these rare instances; however, associated plasticity is very commonly used to model plastic behavior in materials and, therefore, can be regarded as an acceptable solution. The associated flow rule still did not prevent the error in just 14 cases out of 149 billion (1 in 10.6 billion), where radial return was used to find a valid stress state within the yield surface.

Table 1: Occurrences of associated flow and radial return

TSSFAC	Stress Computations	Associated Flow	Radial Return
0.6	1.73547e 11	2,409,659 (0.00139%)	35 (2.01675e −8 %)
0.7	1.48783e 11	1,862,589 (0.00125%)	14 (9.40971e −9 %)
0.8	1.30695e 11	3,981,398 (0.00305%)	49,801 (3.81046e −5 %)
0.9	1.15669e 11	9,149,765 (0.00791%)	421,582 (3.64471e −4 %)

Due to the extremely rare occurrence of the radial return, its effect on the overall results of the simulation were negligible for timestep scale factors of 0.6 and 0.7. In industrial use of finite element software, it is quite common to increase the timestep of the simulation, for example by introducing mass scaling or by increasing the timestep scale factor, for faster turn-around times to get results. When increasing the timestep, the probability of not finding a valid solution using non-associated flow increases.

References

[1] Univ.-Prof. Dr.-Ing. habil. Alexander Lion, “Einführung in die Lineare Viskoelastizität,” *Beiträge zur Materialtheorie*, no. 4/07, May-2007.

[2] E. A. de S. Neto, D. Perić, and D. R. J. Owen, *Computational methods for plasticity: theory and applications*. Chichester, West Sussex, UK: Wiley, 2008.

[3] A. Trojanowski, C. Ruiz, and J. Harding, “Thermomechanical Properties of Polymers at High Rates of Strain,” *J. Phys. IV*, vol. 07, no. C3, pp. C3-447-C3-452, Aug. 1997, doi: 10.1051/jp4:1997377.

[4] W. S. Farren and G. I. Taylor, “The heat developed during plastic extension of metals,” p. 30, Nov. 1924.

[5] G. I. Taylor and H. Quinney, “The Latent Energy Remaining in a Metal after Cold Working,” *Proc. R. Soc. Math. Phys. Eng. Sci.*, vol. 143, no. 849, pp. 307–326, Jan. 1934, doi: 10.1098/rspa.1934.0004.

[6] D. Rittel, “On the conversion of plastic work to heat during high strain rate deformation of glassy polymers,” *Mech. Mater.*, vol. 31, no. 2, pp. 131–139, Feb. 1999, doi: 10.1016/S0167-6636(98)00063-5.

[7] A. Matzenmiller, J. Lubliner, and R. L. Taylor, “A constitutive model for anisotropic damage in fiber-composites,” *Mech. Mater.*, vol. 20, no. 2, pp. 125–152, Apr. 1995, doi: 10.1016/0167-6636(94)00053-0.

[8] Lemaitre, Jean and Desmorat, Rodrigue, *Engineering damage mechanics: ductile, creep, fatigue and brittle failures*. Springer Science & Business Media, 2005.

[9] R. K. Goldberg, K. S. Carney, P. DuBois, C. Hoffarth, S. Rajan, and G. Blackenhorn, “Incorporation of Plasticity and Damage Into an Orthotropic Three-Dimensional Model with Tabulated Input Suitable for Use in Composite Impact Problems,” 2015.

[10] T. Ogasawara, T. Ishikawa, T. Yokozeki, T. Shiraishi, and N. Watanabe, “Effect of on-axis tensile loading on shear properties of an orthogonal 3D woven SiC/SiC composite,” *Compos. Sci. Technol.*, vol. 65, no. 15–16, pp. 2541–2549, Dec. 2005, doi: 10.1016/j.compscitech.2005.06.003.

[11] M. Salavatian and L. V. Smith, “The effect of transverse damage on the shear response of fiber reinforced laminates,” *Compos. Sci. Technol.*, vol. 95, pp. 44–49, May 2014, doi: 10.1016/j.compscitech.2014.02.012.

[12] R. K. Goldberg, K. S. Carney, P. DuBois, C. Hoffarth, S. Rajan, and G. Blankenhorn, “Analysis and Characterization of Damage Utilizing an Orthotropic Generalized Composite Material Model Suitable for Use in Impact Problems,” 2016.

[13] R. K. Goldberg *et al.*, “Incorporation of Failure Into an Orthotropic Three-Dimensional Model with Tabulated Input Suitable for Use in Composite Impact Problems,” 2017.

[14] T. Achstetter, “Development of a Composite Material Shell-Element Model for Impact Applications.” George Mason University, Dec-2019.